Microstructural, Electrical and Magnetic Properties of Erbium Doped Zinc Oxide Single Crystals

P. P. Murmu,[1,2] J. Kennedy,[1,2,*] B. J. Ruck,[2] and S. Rubanov[3]

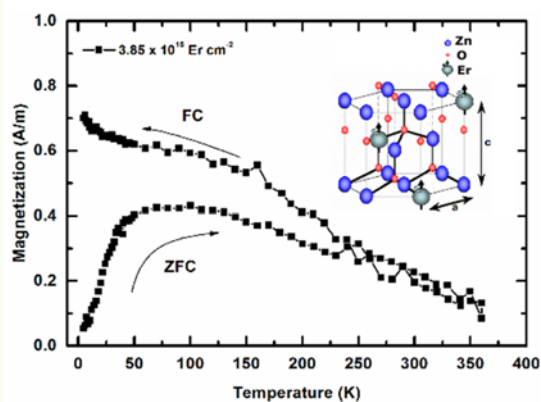[1]National Isotope Centre, GNS Science, PO Box 31312, Lower Hutt 5010, New Zealand
[2]The MacDiarmid Institute for Advanced Materials and Nanotechnology, P.O. Box 600, Wellington 6140, New Zealand
[3]University of Melbourne, Inst Bio21, Melbourne, Vic 3010, Australia

We report the structural, electrical and magnetic properties of erbium (Er) implanted zinc oxide (ZnO) single crystals. Rutherford backscattering and channeling results showed that the majority of Er atoms resided in Zn substitutional lattice sites. Annealing led to a fraction of Er atoms moving into random interstitial sites. Transmission electron microscopy micrographs revealed that doped Er atoms were located in the near-surface region, consistent with the results obtained from DYNAMIC-TRIM calculations. A non-linear Hall-voltage was observed near 100 K, which is associated with inhomogeneous transport in the material. The Er implanted and annealed ZnO exhibited persistent magnetic ordering to room temperature. Ferromagnetism was likely from the presence of intrinsic defects in ZnO, which mediates the magnetic ordering in Er implanted and annealed ZnO.

Keywords: ZnO, erbium, implantation, RBS and channeling, Hall-effect, ferromagnetism

1. INTRODUCTION

Rare-earth doping of zinc oxide (ZnO) is coveted because of its potential applications in optoelectronic devices. ZnO is a direct, wide band gap semiconductor that possesses a large exciton binding energy with potential applications in short-wavelength light emitting devices, sensors and solar cells.[1-8] The optical properties of rare-earth doped ZnO (RE:ZnO) benefit from the intra-*4f* shell transitions of the rare-earth ions, which emit radiation ranging from infra-red to UV. ZnO has been reported to exhibit magnetic ordering upon doping with suitable magnetic ions such as transition metals or rare-earth ions.[1-5] Rare-earth doping of ZnO can thus be highly beneficial in enhancing the functionality of devices by combining optoelectronic and magnetic properties.

Magnetic ordering has been reported in these systems, although universal consensus on the origin of the ferro-magnetism is still reserved. In RE:ZnO systems, carrier-mediated ferromagnetic ordering can occur from coupling between localized dopant *4f* and host *s* electrons. Assadi *et al.*[9] reported that Eu ions can exhibit magnetic coupling provided they are located in the nearest neighbor sites. Shi *et al.*[10] suggested that the magnetic ordering in Gd doped ZnO can be established by electron doping. However, Bantounas *et al.*[11] reported an absence of any long-range magnetic ordering in a similar system. Recently, Venkatesh *et al.*[12] reported ferromagnetic coupling in Gd doped ZnO thin films mediated by a defect band. The defect band was believed to originate from oxygen vacancy related defects, which are needed along with Gd and localized charge carriers, to establish the magnetic ordering in such a system.

Erbium (Er) doped ZnO has traditionally been studied for its well-known optical transition at 1.54 μm. This, in

addition to high conductivity and transparency, makes it of interest for optical devices such as light-emitting diodes, laser diodes and laser amplifiers.[13] Er has been shown to predominantly occupy Zn substitutional lattice sites that may lead to certain optical transitions seen in photoluminescence studies.[14] Er doped ZnO is also a promising dilute magnetic semiconductor for spintronic applications. Magnetic coupling has been reported in this system and has been assigned to many factors, including native defects and metallic segregation.[15,16] These observations suggest that the location of doped ions and their surroundings in the host matrix greatly influence the material's properties and demand a more detailed examination of their fundamental and technological applications. In this paper, we report the microstructural, electrical and magnetic results from Er implanted and annealed ZnO single crystals. Room temperature ferromagnetism was observed in Er implanted and annealed ZnO. This phenomenon is explained experimentally.

2. EXPERIMENTAL PROCEDURE

Hydrothermally grown ZnO (0001) single crystals (Semi-wafer Inc.) were doped using the ion implanter at the GNS Science low-energy ion implanter facility.[17] 40 keV Er implantation was carried out at ambient temperature for fluences ranging from 6.65×10^{14} to 1.1×10^{16} Er cm^{-2}. Elemental depth profiles were obtained from DYNAMIC-TRIM calculations and the average depth of the implanted ions was approximately 12 nm.[18,19] Unimplanted and Er implanted ZnO samples were annealed at 650°C for 30 minutes under high vacuum ($\sim 1 \times 10^{-7}$ mbar). Rutherford backscattering spectrometry under channeling condition (RBS channeling) measurements were conducted using a 1 mm collimated 2 MeV He$^+$ beam.[20] The microstructural properties of the samples were investigated using transmission electron microscopy (TEM). The TEM measurements and energy-filtered TEM (EFTEM) imaging were performed using FEI TECNAI TF20 field emission gun transmission electron microscopes and JEOL, JEM-2100 (using 11Mpix CCD camera (Gatan, Orius1000)) operating at 200 kV. Electrical and magnetic properties were studied using a physical property measurement system (PPMS) and super-conducting quantum interference device (SQUID) magnetometer from Quantum Design, respectively. Also, element specific x-ray absorption near edge spectra (XANES) experiments were carried out at the Australian synchrotron soft x-ray beam-line. The spectra were collected at the O K-edge in total electron yield (TEY) mode.[21]

3. RESULTS AND DISCUSSION

RBS and channeling measurements were carried out to assess the crystalline quality and to investigate the incorporation

of the Er atoms in the ZnO lattice. The Er location in the ZnO sub-lattice was investigated by performing angle dependent RBS/C measurements around the [0001]-axis. Figure 1 shows angular scans for 6.65×10^{14} Er cm^{-2} as-implanted and 650°C annealed ZnO single crystals, along with a 6.4×10^{15} Er cm^{-2} implanted and 650°C annealed ZnO single crystal. Angular scan profiles for Zn and Er showed a similar trend, suggesting both are subjected to similar disorder. The fraction of Er atoms in the Zn sub-lattice was estimated using $(1 - {}^{Er}\chi_{min})/(1 - {}^{Zn}\chi_{min})$, where ${}^{Er}\chi_{min}$ and ${}^{Zn}\chi_{min}$ are the χ_{min} values associated with Er and Zn, respectively.[22] For as-implanted ZnO:Er implanted with 6.65×10^{14} Er cm^{-2}, around 92% of the Er atoms were estimated to occupy Zn substitutional lattice sites. It should be noted that, as for Gd implantation, a fraction of the Er atoms may also reside interstitially, but are shadowed by columns along the c-axis.[20] After annealing the sample at 650°C, around 82% of the Er atoms still occupy substitutional lattice sites. For a 6.4×10^{15} Er cm^{-2} implanted and 650°C annealed ZnO single crystal, the fraction of substitutionally located Er atoms decreased to ~40%. It is clear that, in low fluence as-implanted ZnO, the majority of Er atoms are located in substitutional lattice sites. A similar trend was observed by Alves *et al.*,[14] who suggested that complete damage recovery can be achieved by annealing the sample at 1050°C.

The microstructural properties of Er implanted and annealed ZnO were examined using TEM. Figure 2 presents micrographs showing zero-loss (elastic) and EFTEM elemental maps associated with Er, Zn, and O for a 3.85×10^{15} Er cm^{-2} implanted and 650°C annealed ZnO single crystal. The EFTEM micrograph for Er atoms in Fig. 2(b) revealed a bright white strip near the sample surface, indicating that Er atoms are located in the implanted region at a depth of ~10 nm. No distinct change in Zn and O maps
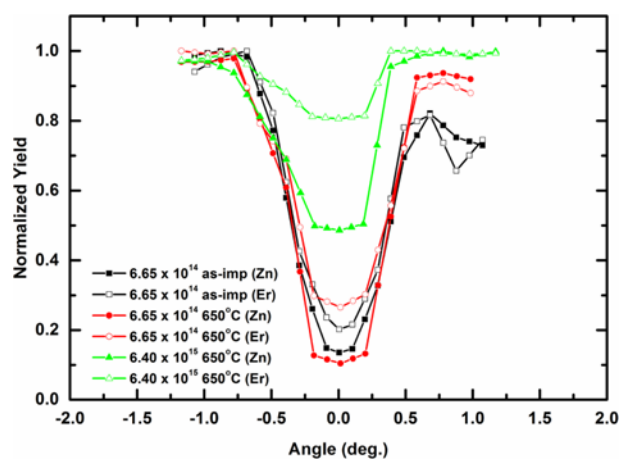

Fig. 1. Angular scans along [0001]-direction measured for 6.65×10^{14} and 6.4×10^{15} Er cm^{-2} implanted and 650°C annealed ZnO single crystals.
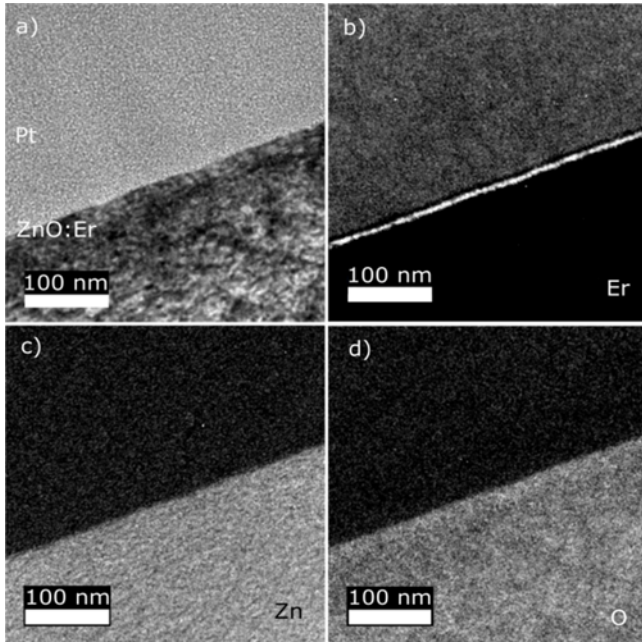
Fig. 2. (a) Zero-loss (elastic) TEM, and EFTEM elemental maps for (b) Er (c) Zn and (d) O for a 3.85×10^{15} Er cm^{-2} implanted and 650°C annealed ZnO single crystal.
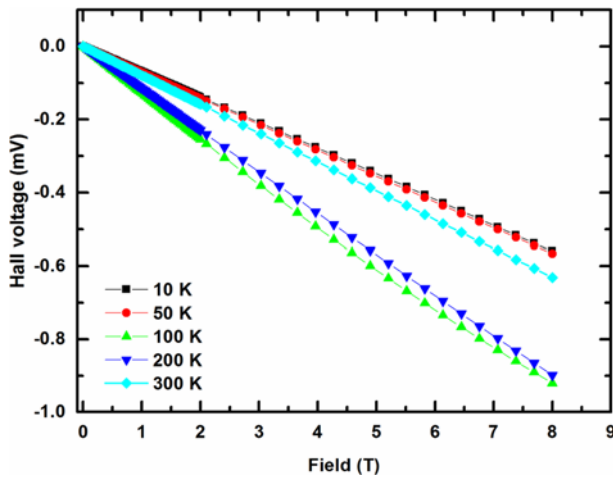

Fig. 3. Field dependent Hall-voltage for a 6.4×10^{15} Er cm^{-2} implanted and 650°C annealed ZnO single crystal.
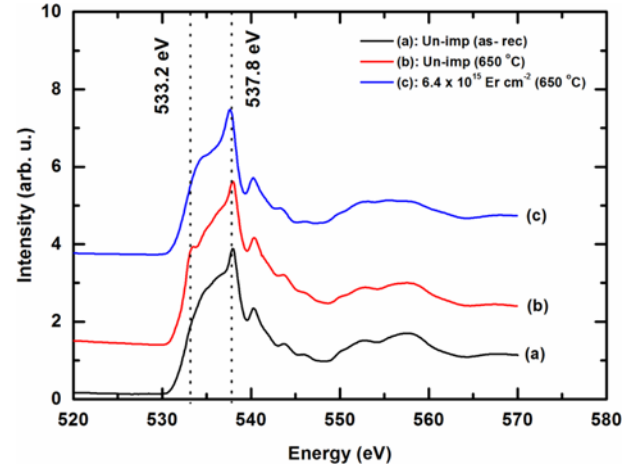

Fig. 4. XANES spectra of O K-edge for un-implanted (a) as-received, (b) 650°C and (c) 6.4×10^{15} Er cm^{-2} implanted and 650°C annealed ZnO single crystals (spectra vertically offset for clarity).

close to the surface was observed and the results were similar to those observed for similar fluences of Gd implanted into ZnO.[21]

Figure 3 shows the magnetic field dependent Hall-voltage for a 6.4×10^{15} Er cm^{-2} implanted and 650°C annealed ZnO single crystal. Hall-voltages from 10 to 300 K exhibited a linear dependence with a negative slope, indicating that electrons are the major charge carriers. The room temperature data suggest a carrier concentration of approximately 6×10^{19} cm^{-3}, which was calculated assuming conduction in the top 40 nm of the film. The slopes of the Hall voltage for the 100 K and 200 K curves in Fig. 3 are larger than the slopes for curves at 10 K, 50 K and 300 K. It is evident that the carrier concentration decreased from 300 K to 100 K, below which the carrier concentration increased again. A non-linear Hall-voltage was observed at around 100 K. A similar trend was observed in Gd implanted and annealed ZnO single crystals, which is believed to be from non-homogenous transport in the material.[23] Er implantation and annealing also resulted in ZnO:Er showing characteristics of a heavily doped degenerate semiconductor.

The electronic properties of Er implanted and annealed ZnO were investigated using x-ray absorption near edge spectroscopy (XANES). Figure 4 shows the O K-edge XANES for un-implanted and 6.4×10^{15} Er cm^{-2} and 650°C ZnO single crystals, which also included the O K-edge XANES for an as-deposited ZnO film. The main peak at ~537.8 eV was attributed to electronic transitions from O 1s to un-occupied p-like states. Unlike in the annealed ZnO single crystal and the as-deposited film,[21] no pre-edge features were observed in Er implanted and annealed ZnO, and their spectra were similar to the as-received ZnO.

The pre-edges features have been suggested to originate from oxygen vacancy related defect states,[24] although other intrinsic defects cannot be ruled out. In Er implanted and annealed ZnO single crystals, oxygen vacancies may be compensated by some mechanism resulting in no pre-edge features. RBS/C results indicated that annealing drove out Er atoms from substitutional to random interstitial sites. A fraction of Er may even end up at oxygen vacancies, which can suppress any features associated with oxygen vacancies. This is similar to the report of Pereira *et al.*[25] who found Co and Mn acquired antisite lattice sites in ZnO. Only a small concentration is likely to be required to compensate oxygen vacancies in ZnO.[23]
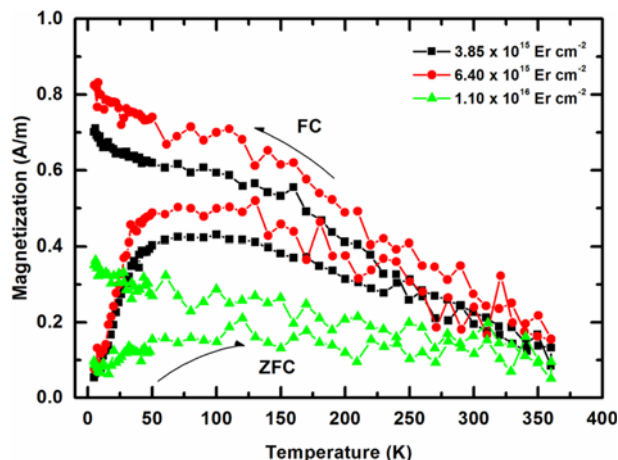
Fig. 5. M(T) curves for Er implanted and 650°C annealed ZnO single crystals. FC/ZFC measurements were performed at an applied field of 10 mT.

Temperature dependent magnetization, M(T), curves were obtained to investigate the magnetic transition temperatures. Field-cooled (FC) and zero-field cooled (ZFC) measurements were performed at 10 mT. FC and ZFC curves for 3.85×10^{15}, 6.4×10^{15} and 1.1×10^{16} Er cm^{-2} implanted and 650°C annealed ZnO single crystals are shown in Fig. 5. The FC and ZFC curves showed clear divergence up to room temperature; and the FC curves showed increasing magnetization from 360 K down to 90 K. An upturn was observed below 60 K, which originated from moments in the samples that remained paramagnetic.

From Figure 5 it is evident that Er implanted and annealed ZnO showed room temperature ferromagnetism. It is important to examine the contribution from magnetic Er, Zn and O phases. Er-metal and ErZn are ferromagnetic with $T_C \sim$ 20 K,[26,27] whereas Er_2O_3 is antiferromagnetic with $T_N \sim$ 3.3 K.[28] Er-metal, ErZn and Er_2O_3 can thus be excluded as the sources of room temperature ferromagnetism in ZnO:Er samples. The similarity of the FC/ZFC curves at higher temperatures suggests that ZnO:Er contains superparamagnetic nanoparticles. Er-rich nano-sized inclusions are likely to form in Er implanted and annealed ZnO, as seen in the EFTEM micrographs in Fig. 2. These inclusions must have a relatively wide size distribution because no distinct blocking temperature, T_B, was observed in the ZFC curves. The FC curves suggest that both ferromagnetic and paramagnetic phases contribute to the magnetization. Non-uniformly distributed Er atoms are likely to show ferromagnetic and paramagnetic interactions from substitutional and randomly distributed Er atoms in ZnO. A similar trend was reported in Co doped ZnO, which exhibited a ferromagnetic signal along with paramagnetic ordering from substitutional and random Co atoms, respectively.[29] However, care must be taken to associate magnetic properties to Er atoms in ZnO:Er because ferromagnetism is also seen in un-implanted and

annealed ZnO.[23] Recently, Venkatesh *et al.*[12] observed magnetic ordering in Gd doped ZnO films mediated by a defect-band. The defect band can be associated with doped ions (Gd in this case) or with intrinsic defects such as oxygen vacancies. The observation of magnetic ordering in undoped ZnO in our previous study also suggests that the intrinsic defects play a crucial role in establishing the ferromagnetism.[23]

4. CONCLUSIONS

In conclusion, the microstructural, electronic, electrical and magnetic properties of erbium implanted ZnO single crystals were investigated. RBS and channeling results showed that for low-fluence implanted ZnO the majority of the Er atoms were located in Zn substitutional lattice sites. Annealing was found to drive out a fraction of Er atoms into the random interstitials sites. The microstructural analysis indicated that the Er atoms were located in the near-surface region, consistent with predictions from DYNAMIC-TRIM calculations. Hall-voltage showed a non-linear behavior at 100 K that was from inhomogeneous transport in the sample. XANES results did not show any pre-edge feature on the O-K edge for Er implanted and annealed ZnO, suggesting the compensation of intrinsic defects responsible for the feature. The observed room temperature ferromagnetism was likely to be established by intrinsic defects in Er implanted and annealed ZnO.

REFERENCES

1. C. Liu, F. Yun, and H. Morkoç, *J. Mater. Sci-Mater. El.* **16**, 555 (2005).
2. M. Tay, Y. H. Wu, G. C. Han, Y. B. Chen, X. Q. Pan, S. J. Wang, P. Yang, and Y. P. Feng, *J. Mater. Sci-Mater. El.* **20**, 60 (2009).
3. S. Kang, Y. Kim, S. E. Kim, and S. Kim, *Electron. Mater. Lett.* **9**, 7 (2013).
4. S. Chawla, M. Saroha, and R. K. Kotnala, *Electron. Mater. Lett.* **10**, 73 (2014).
5. D. E. Motaung, I. Kortidis, D. Papadaki, S. S. Nkosi, G. H. Mhlongo, J. Wesley-Smith, G. F. Malgas, B. W. Mwaki-kunga, E. Coetsee, H. C. Swart, G. Kiriakidis, and S. S. Ray, *Appl. Surf. Sci.* **311**, 14 (2014).

6. G. H. Mhlongo, D. E. Motaung, S. S. Nkosi, H. C. Swart, G. F. Malgas, T. K. Hillie, and B. W. Mwakikunga, *Appl. Surf. Sci.* **293**, 62 (2014).

7. G. F. Malgas, D. E. Motaung, S. S. Nkosi, G. H. Mhlongo, B. W. Mwakikunga, C. J. Arendse, and T. F. G. Muller, *Thin Solid Films* **555**, 100 (2014).

8. H. Kunert, M. Govender, A. Machatine, B. Mwakikunga, and P. Niyongabo, *Phys. Status Solidi (a)* **211**, 435 (2014).

9. M. H. N. Assadi, Y. Zhang, R. K. Zheng, S. P. Ringer, and S. Li, *Nanoscale Res. Lett.* **6**, 357 (2011).

10. H. Shi, P. Zhang, S. S. Li, and J. B. Xia, *J. Appl. Phys.* **106**, 023910 (2009).

11. I. Bantounas, S. Goumri-Said, M. B. Kanoun, A. Manchon, I. Roqan, and U. Schwingenschlögl, *J. Appl. Phys.* **109**, 083929 (2011).

12. S. Venkatesh, J. B. Franklin, M. P. Ryan, J. S. Lee, H. Ohldag, M. A. McLachlan, N. M. Alford, and I. S. Roqan, *J. Appl. Phys.* **117**, 013913 (2015).

13. A. K. Pradhan, L. Douglas, H. Mustafa, R. Mundle, D. Hunter, and C. E. Bonner, *Appl. Phys. Lett.* **90**, 072108 (2007).

14. E. Alves, E. Rita, U. Wahl, J. G. Correia, T. Monteiro, J. Soares, and C. Boemare, *Nucl. Instrum. Meth. B* **206**, 1047 (2003).

15. J. Qi, Y. Yang, L. Zhang, J. Chi, D. Gao, and D. Xue, *Scripta Mater.* **60**, 289 (2009).

16. H. M. Chen, X. C. Liu, S. Y. Zhuo, Z. Xiong, R. W. Zhou, F. Li, and E. W. Shi, *AIP Adv.* **4**, 047121 (2014).

17. J. Kennedy, J. Leveneur, G. V. M. Williams, D. R. G. Mitchell, and A. Markwitz, *Nanotechnology* **22**, 115602 (2011).

18. J. P. Biersack, *Nucl. Instrum. Meth. B* **27**, 21 (1987).

19. P. P. Murmu, J. Kennedy, B. J. Ruck, A. Markwitz, G. V. M. Williams, and S. Rubanov, *Nucl. Instrum. Meth. B* **272**, 100 (2012).

20. P. P. Murmu, R. J. Mendelsberg, J. Kennedy, D. A. Carder, B. J. Ruck, A. Markwitz, R. J. Reeves, P. Malar, and T. Osipowicz, *J. Appl. Phys.* **110**, 033534 (2011).

21. P. P. Murmu, J. Kennedy, B. J. Ruck, G. V. M. Williams, A. Markwitz, S. Rubanov, and A. A. Suvorova, *J. Mater. Sci.* **47**, 1119 (2012).

22. J. R. Tesmer and M. Nastasi, *Handbook for Modern Ion Beam Analysis*, p. 274, Materials Research Society, Pittsburgh (1995).

23. J. Kennedy, G. V. M. Williams, P. P. Murmu, and B. J. Ruck, *Phys. Rev. B* **88**, 214423 (2013).

24. A. P. Singh, R. Kumar, P. Thakur, N. B. Brookes, K. H. Chae, and W. K. Choi, *J. Phys.-Condens. Mat.* **21**, 185005 (2009).

25. L. M. C. Pereira, U. Wahl, S. Decoster, J. G. Correia, L. M. Amorim, M. R. da Silva, J. P. Araujo, and A. Vantomme, *Phys. Rev. B* **84**, 125204 (2011).

26. J. F. Elliott, S. Legvold, and F. H. Spedding, *Phys. Rev.* **100**, 1595 (1955).

27. P. Morin, J. Rouchy, and E. du Tremolet de Lacheisserie, *Phys. Rev. B* **16**, 3182 (1977).

28. Y. J. Tang, X. W. Cao, J. C. Ho, and H. C. Ku, *Phys. Rev. B* **46**, 1213 (1992).

29. B. Martinez, F. Sandiumenge, L. Balcells, J. Arbiol, F. Sibieude, and C. Monty, *Phys. Rev. B* **72**, 165202 (2005).